Heliyon 10 (2024) e24003

Contents lists available at ScienceDirect

Heliyon

journal homepage: www.cell.com/heliyon

Two typical phases of failure acceleration in rocks under uniaxial compression

Lei Cheng [a], Shengwang Hao [a,*], Chunsheng Lu [b], Sunji Zhou [a]

[a] School of Civil Engineering and Mechanics, Yanshan University, Qinhuangdao, 066004, China
[b] School of Civil and Mechanical Engineering, Curtin University, Perth, Western Australia, 6845, Australia

ARTICLE INFO

Keywords:
Precursory acceleration
Catastrophic failure
Rocks
Failure time
Prediction

ABSTRACT

The critical power-law acceleration of response quantities has been widely accepted and validated as an effective way to predict the failure time. However, in practical applications, only the data in the vicinity of the failure time exhibit critical power-law behaviour, which cannot describe the entire acceleration stage. In this study, it is shown that by using experimental results from the catastrophic failure of rocks under uniaxial compression, the acceleration of the mean strain presents two typical phases, and the final data in close proximity to the catastrophic time conform to the critical power-law trend. The early part of the acceleration stage is dominated by an exponential relationship with time to failure. Thus, the entire acceleration stage can be described using a combination of exponential and power-law functions. A prediction method based on a combined description of the entire acceleration failure process is proposed to forecast the failure time and is validated by experimental results. This combined description allows for an earlier warning of catastrophic failure than the power-law alone.

1. Introduction

The catastrophic failure of heterogeneous materials has attracted significant interest owing to its similarity to disasters occurring in manmade and natural structures [1–5]. It has been revealed that the accelerating trend of strain and other response quantities approaching catastrophic time is a precursor to catastrophic failure [1,4,6–12]. These acceleration precursors have been observed before natural disasters [6,8,10–12] and during failure experiments [9,13–18]. Such a critical acceleration process of the response rates can be described by the following power-law relationship [1,6,9,11,13–19]:

$$\dot{\Omega} = B(t_F - t)^{-\beta} \tag{1}$$

where Ω represents a response quantity, and the dot above it refers to differentiation with respect to time, t; t_F is the failure time; β is the critical power-law exponent; and B is a constant. Eq. (1) can be deduced from the well-known Voight relation [6,19], which describes the failure acceleration of materials with $k = [A\ (\alpha - 1)]^{1/(1-\alpha)}$ and $\beta = 1/(\alpha - 1)$ [19]:

$$\dot{\Omega}^{-\ \alpha}\ \ddot{\Omega}\ \ - A = 0 \tag{2}$$

where α indicates the degree of acceleration, and A is a constant.

* Corresponding author.
E-mail address: hsw@ysu.edu.cn (S. Hao).

https://doi.org/10.1016/j.heliyon.2024.e24003
Received 12 July 2023; Received in revised form 7 October 2023; Accepted 2 January 2024
Available online 3 January 2024
2405-8440/© 2024 The Authors. Published by Elsevier Ltd. This is an open access article under the CC BY-NC-ND license (http://creativecommons.org/licenses/by-nc-nd/4.0/).

Eq. (1) can be rewritten in linearised form as follows [15,20]:

$$\dot{\Omega}^{-1/\beta} = B^{-1/\beta}\,(t_F - t) \tag{3}$$

The failure time can be predicted by extrapolating the line from a plot of $\dot{\Omega}^{-1/\beta}$ versus t to the time point of $\dot{\Omega}^{-1/\beta} = 0$. The critical power-law acceleration behaviour (Eq. (1)) of the response functions close to the catastrophic failure point have been demonstrated in rock experiments [16,18], elastic-brittle materials [21], and ceramic coating systems [7,9]. Such a failure-forecasting method [15,20,22,23] has been confirmed by the retrospective prediction of failures in laboratory experiments [4,9,13,16–18], landslides [8,12], volcanic eruptions [6,20,22–24], and structural health monitoring [25]. Several attempts have been made to assess and increase the accuracy of this method for forecasting failures in real time [14–16,20,26–28]. However, it should be noted that in practical applications, only data in the vicinity of the failure time can exhibit critical behaviour [20]. The prediction results of Hao et al. [20], based on the "cumulative time technique" and "simple moving time window technique", showed that the earlier data that deviate significantly from the final power-law behaviour have a significant influence on the accuracy of predictions. The inverse power-law used to forecast failure time only applies near failure [11]. The test results of Vasseur et al. [29], using Bayesian Criterion Information, indicated that the first stages of deformation acceleration generally follow an exponential trend. Considerable experimental and theoretical studies and field observations have focused on critical power-law behaviour, but a full understanding of the entire acceleration stage during failure is still lacking.

In this study, quasi-static and uniaxial compression experiments were conducted on three types of rocks (sandstone, granite, and marble) to simulate the energy release driving catastrophic failure and to investigate the acceleration process of failure. We found that the acceleration stage includes two phases: the evolving trend of the earlier data in the first phase of the acceleration stage is dominated by an exponential relationship with the time to failure, and the data in the second phase, close to the failure time, evolve according to the power-law behaviour of Eq. (1). The entire acceleration process of the strain rates can be described using a combination of exponential and power-law functions. Based on this description, a method is proposed for predicting the catastrophic failure time.

2. Experiments and methods

In the laboratory tests, the load apparatus and tested rock samples were both deformed during compression in series. This is usually modelled using the system illustrated in Fig. 1a. The "elastic spring" represents the load apparatus, and k is the stiffness of the elastic spring. Thus, the compressive displacement U of the testing machine crosshead combines the deformation of the loading apparatus and the deformation u of the rock sample (Fig. 1a).

Three types of rocks (grey sandstone, brown marble, and black granite) were cut into prism-shaped blocks 40 mm in height and 16 × 20 mm^2 in cross-section. To decrease or eliminate the end effect, the height of the specimen was larger than or equal to double the width, and the top and bottom contact surfaces of the rock specimen with the load plate were buttered during the tests. Fig. 2 shows the

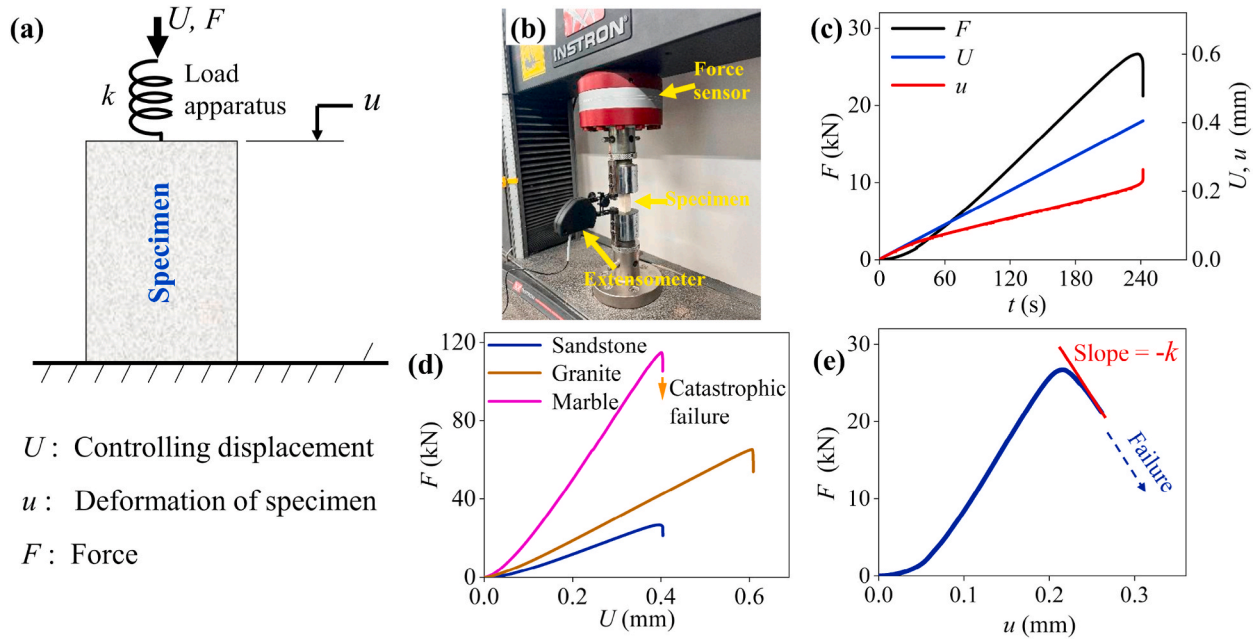

Fig. 1. Experimental setup, samples, and evolutions of F, U, and u. (a) Schematic of the uniaxial compression system. The elastic spring represents the load apparatus. (b) Testing equipment for uniaxial compression tests. (c) Evolutions of F, U, and u. (d) F–U curves for three types of rocks. (e) Representative experimental result showing the critical condition (Eq. (9)) of catastrophic failure.

internal microstructures in the scanning electron micrographs of the three rock types. All rock samples were compressed uniaxially along the height axis using an Instron 5982 testing machine (Instron, Norwood, MA, USA) at a constant crosshead speed (Fig. 1b), so U increased linearly with time (Fig. 1c). Consequently, the load apparatus of the test machine accumulated substantial elastic energy during deformation. A total of 25 specimens of each rock type were tested. The representative results for the three rock types are shown in Fig. 1. After the peak stress, the load apparatus releases the stored deformation energy, which may trigger catastrophic failure of the rock sample (Fig. 1c–e).

The deformation, u, of a rock sample was monitored using an extensometer located on its side, which had a 1 μm resolution (Fig. 1b). Force was measured using a force sensor (Fig. 1b) with an offset load of 1 kN. The load curves of the three rock types show a clear post-peak phase (Fig. 1d). This indicates that these rocks can deform stably after the peak force and exhibit a stress-softening behaviour. The experiments show that u exhibits an accelerating evolution that finally leads to catastrophic failure (Fig. 1c–e). A catastrophic failure point appeared in the stress-softening stage after the peak force.

3. Theoretical analysis of catastrophic failure

To analyse catastrophic instability, let us consider a spring-sample system (Fig. 1a) loaded by controlling the boundary displacement, U. The instability of this system is determined by the stiffness (k) of the elastic spring and the post-failure evolving behaviours of the rock sample. Following the peak or maximum force, an increment ($\mathrm{d}U$) in the boundary load displacement produces an increment ($\mathrm{d}u$) in the sample's deformation, but a decrement ($\mathrm{d}F$) in the external force, F. Stress-softening results in a recovery $\mathrm{d}u_e = \mathrm{d}F/k$ in the deformation, u_e, of the elastic spring. The value of $\mathrm{d}u_e$ is negative because $\mathrm{d}F$ is negative after the peak force, corresponding to the reduction of F with increasing displacement of U.

In this process, the external force changes from F to $F + \mathrm{d}F$, induced by an increase in the boundary displacement, $\mathrm{d}U$, and the external work, $\mathrm{d}W$, created by the external load can be calculated as follows:

$$\mathrm{d}W = (F + \mathrm{d}F/2)\mathrm{d}U \tag{4}$$

During the deformation process after the peak force, the deformation stability is governed by three types of energies: the increment of the external work $\mathrm{d}W$ done by the external load, and the energy release from the elastic spring

$$\mathrm{d}W_e = -(F + \mathrm{d}F/2)\mathrm{d}u_e \tag{5}$$

owing to its deformation recovery ($\mathrm{d}u_e$) and the required work

$$\mathrm{d}W_d = (F + \mathrm{d}F/2)\mathrm{d}u \tag{6}$$

to produce a deformation increment $\mathrm{d}u$ in the rock sample.

Deformation instability occurs in the spring-sample system (Fig. 1a) when the energy released from the elastic spring ($\mathrm{d}W_e$) compensates for or is larger than the required work ($\mathrm{d}W_d$), inducing a deformation increment $\mathrm{d}u$ in the rock sample. Consequently, without any external input, failure (or deformation) proceeds self-sustainably and uncontrollably in a rock sample. Therefore, the deformation is stable only when

$$\mathrm{d}W_e < \mathrm{d}W_d \tag{7}$$

Substituting Eqs. (5) and (6) into Eq. (7) gives

$$-\mathrm{d}u_e = -\mathrm{d}F/k < \mathrm{d}u = \mathrm{d}F/(\mathrm{d}F/\mathrm{d}u) \tag{8}$$

In Eq. (8), the stiffness of the elastic spring is larger than the negative value of the slope of the tangent of the force-deformation curve of the rock sample, that is $k > -\mathrm{d}F/\mathrm{du}$. The critical conditions driving the catastrophic failure in the rock sample are shown in (Fig. 1e), where

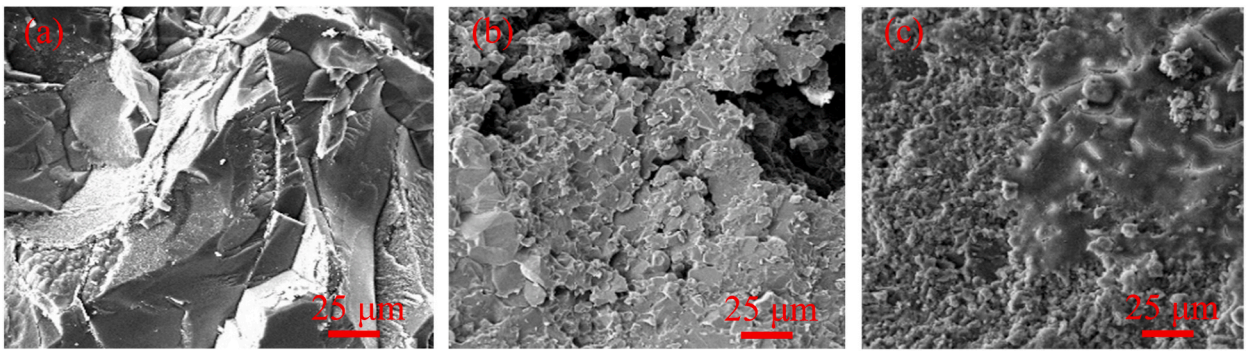

Fig. 2. Scanning electron micrographs of three types of rocks: (a) granite, (b) sandstone, and (c) marble.

$$dF / du = -k \tag{9}$$

The external force on the elastic spring, shown in Fig. 1a, can be expressed as follows:

$$F = ku_e \tag{10}$$

The deformation of the elastic spring is the difference between the boundary displacement, U, and the sample deformation, u:

$$u_e = U - u \tag{11}$$

Eqs. (10) and (11) result in

$$F = k(U - u) \tag{12}$$

Differentiation of Eq. (12) with respect to u yields

$$dF / du = k dU/du - k \tag{13}$$

Eqs. (9) and (13) indicate that the critical condition for catastrophic instability can be expressed as

$$dU / du = 0 \text{ or } du / dU \to \infty \tag{14}$$

Therefore, the relative response rate, du/dU, of the deformation (u) with respect to the control variable (U) tended to exhibit singularity at the catastrophic point. Consequently, the catastrophic failure point is defined as the time point when the relative response rate is $du/dU \to \infty$.

Catastrophic instability can also be represented as an increment, du, in the deformation of the rock sample induced by the energy release, dW, of the elastic spring without external work input. This is expressed as follows:

$$dW / du = 0 \tag{15}$$

Eq. (15) yields the critical condition in Eq. (14).

4. Acceleration process approaching the failure time

Since the critical condition of catastrophic instability of failure is $du/dU \to \infty$ (Eq. (14)), in order to clearly observe the acceleration of deformation rates evolving to the catastrophic failure time, we define a strain response function as the relative change rate of the average strain $\varepsilon = u/l$ with respect to the load displacement (U):

$$R = \frac{d\varepsilon}{dU} \tag{16}$$

where l denotes the height of the sample. The rapid increases of strains, ε (Fig. 3a), and the response function, R (Fig. 3b), approaching the catastrophic failure time illustrates a precursory accelerating trend of the tested samples' deformations. This indicates that the response function R tends toward a singularity (as shown in Eq. (14)), as determined by the energy criterion for the catastrophic instability of failure. The response function, R, represents the relative change of a response variable (the average strain, ε) with respect to the control variable (U). Critical criterion (14) indicates that R, an indicator of the occurrence of catastrophic failure, tends towards infinity. Consequently, a description of the evolving trend of R approaching infinity can predict the time of catastrophe.

To characterise the accelerating properties of the deformations approaching the catastrophic point, Fig. 4 plots the log–log curves of R against the remaining life ($U_F - U$) for three typical rock samples in which catastrophic failure occurs. R and U in the above equation are normalised by their values monitored at the catastrophic failure time in the experiments, that is, R_{max} and U_F, respectively. The

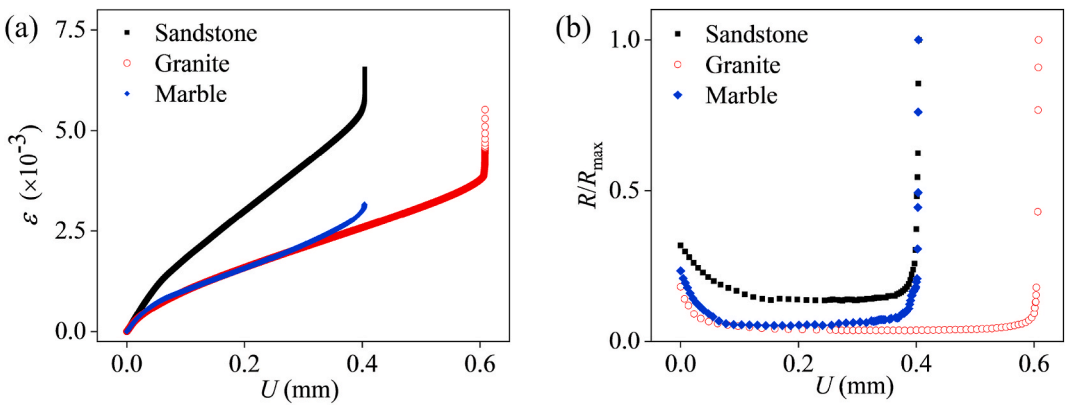

Fig. 3. Evolutions of ε and R for three types of rocks, showing the acceleration of failure.

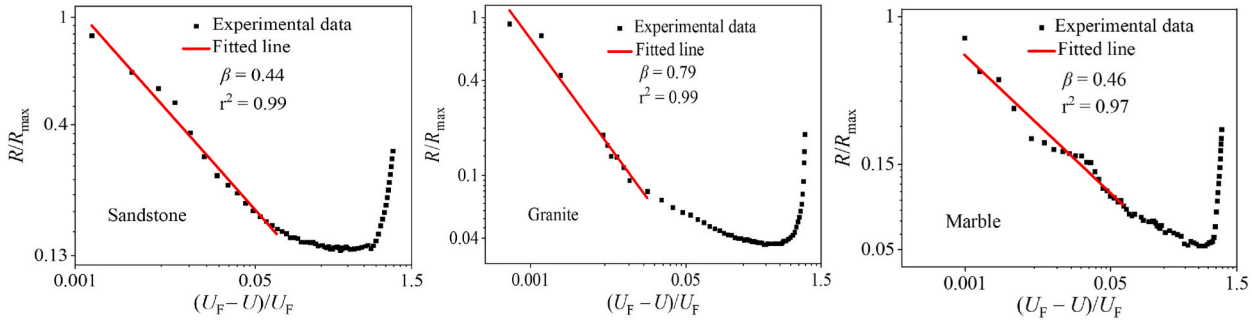

Fig. 4. Double logarithmic curve showing the power-law relationship of Eq. (17).

linear trend of these log–log curves in proximity to the catastrophic failure time indicates that the critical accelerating process of the strain rates follows a power-law relationship:

$$R_a = B(U_F - U)^{-\beta} \tag{17}$$

It should be mentioned that in the experiments U has a linear relationship with t so that Eq. (17) is consistent with Eq. (1). R_a represents the value of R in the acceleration stage to distinguish it from the values of R during the entire loading process.

According to Eq. (17), $R_a^{-1/\beta}$ decreases linearly with U to zero at the catastrophic failure time when $U = U_F$. It should be noted that Eqs. (17) and (18) are interval expressions. To determine the interval range in Figs. 6 and 7, we used a linear fitting technique based on the least-squares method. During the fitting process, the dataset used for fitting was determined according to the principle of maximum correlation coefficient, and as many data points as possible were included [18]. To clearly demonstrate the two phases of the acceleration process, the curves of $R^{-1/\beta}$ versus U are plotted in Fig. 5a, 6a and 7a. The earlier data in the acceleration phase deviate from the linear trend exhibited by the data in the vicinity of the catastrophic failure time. This is identical to the results shown in Fig. 4, where

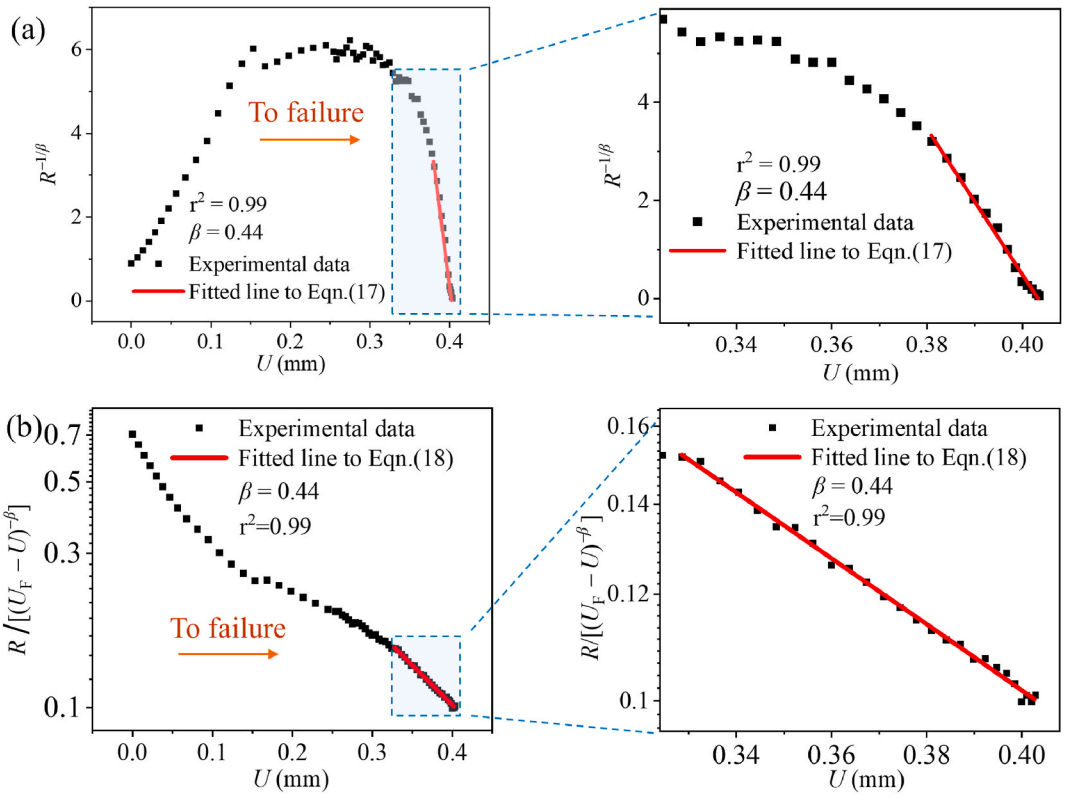

Fig. 5. Evolution of strain rates and description of failure acceleration of a sandstone specimen. (a) $R^{-1/\beta}$ versus U. (b) Logarithmic curves of $R/(U_F - U)^{-}\beta$ versus U. Magnifications of the subplots on the left in the proximity of the failure time are shown in the subplots on the right to enhance the details of the fittings to Eqs. (17) and (18).

only the strain-rate data close to the failure time conform to the power-law behaviour of Eq. (17). The data from the early part of the acceleration stage do not follow the critical power-law tendency. However, the linear parts of the logarithmic curves of $R/(U_F - U)^{-\beta}$ versus U for the three rock types (as shown in Fig. 5b, 6b and 7b) indicate that the entire acceleration stage can be described as

$$R_a = H\exp[-(U_F - U)](U_F - U)^{-\beta} \tag{18}$$

This indicates that in the early part of the acceleration stage, the strain rate is dominated by an exponential relationship with time. The data in the acceleration stage can be described well using a combination of exponential and power-law functions. The other data deviated from the fitted trend.

5. Predicting the failure time based on the description of the whole acceleration process

The combined description of the whole acceleration process of Eq. (18) yields:

$$\log R_a = \log H - (U_F - U) - \beta\log(U_F - U) \tag{19}$$

Differentiation of Eq. (19) with respect to U gives

$$(\dot{R}_a/R_a - 1)^{-1} = \frac{1}{\beta}(U_F - U) \tag{20}$$

where $\dot{R}_a$ is defined as the differentiation of R_a against U, i.e., $\dot{R}_a = d^2\varepsilon/dU^2$. Eq. (20) indicates that $(\dot{R}_a/R_a - 1)^{-1}$ linearly decreases with U. Then, the prediction of U_F can be achieved by linearly extrapolating the curve of $(\dot{R}_a/R_a - 1)^{-1}$ to zero.

Close to the catastrophic point, the values of $\dot{R}_a/R_a$ are large, and the first term on the left side of Eq. (20) is approximated as follows:

$$R_a\dot{R}_a^{-1} = \frac{1}{\beta}(U_F - U) \tag{21}$$

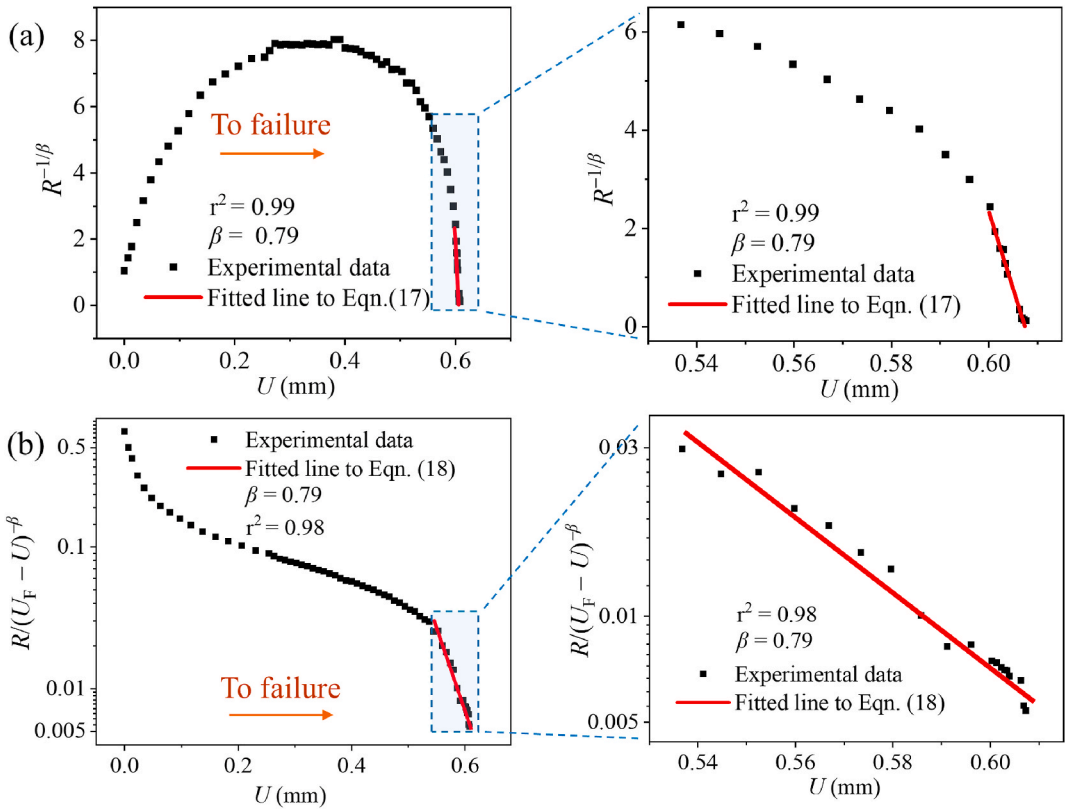

Fig. 6. Evolution of strain rates and description of failure acceleration of a granite specimen. (a) $R^{-1/\beta}$ versus U. (b) Logarithmic curves of $R/(U_F - U)^{-}\beta$ versus U. Magnifications of the subplots on the left in the proximity of the failure time are shown in the subplots on the right to enhance the details of the fittings to Eqs. (17) and (18).

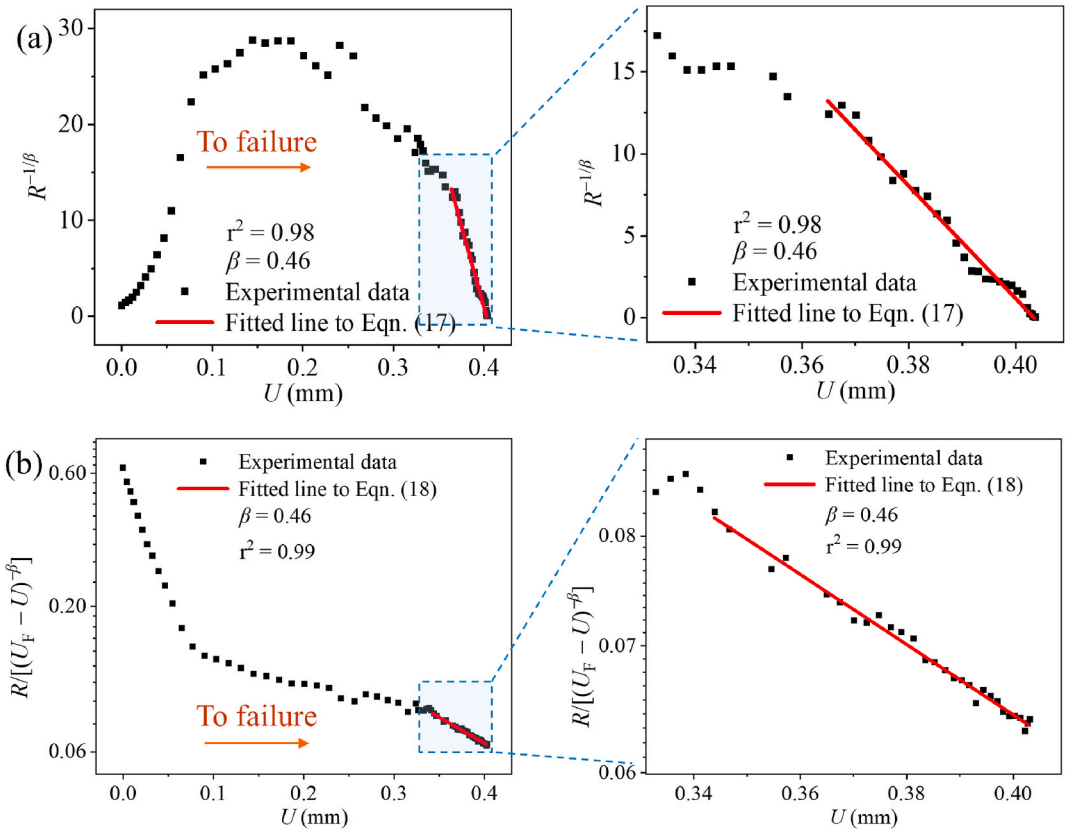

Fig. 7. Evolution of strain rates and description of failure acceleration of a marble specimen. (a) $R^{-1/\beta}$ versus U. (b) Logarithmic curves of $R/(U_F - U)^{-}\beta$ versus U. Magnifications of the subplots on the left in the proximity of the failure time are shown in the subplots on the right to enhance the details of the fittings to Eqs. (17) and (18).

In the experiments, U increased linearly with time t; therefore, Eq. (21) is consistent with the following relationship [20,21]:

$$R_a \dot{R}_a^{-1} = \frac{1}{\beta}(t_F - t) \tag{22}$$

Eqs. (20) and (21) can be verified by the linear behaviour of $(\dot{R}_a / R_a - 1)^{-1}$ and $R_a \dot{R}_a^{-1}$ versus U close to the failure time in the experimental results, as shown in Fig. 8. It is evident that close to the failure time, there is little difference between the experimental

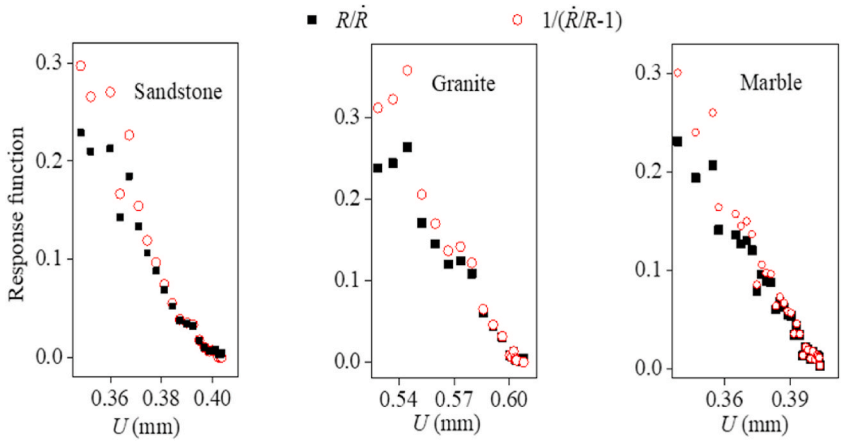

Fig. 8. Experimental data of $(\dot{R}_a / R_a - 1)^{-1}$ and $R_a \dot{R}_a^{-1}$ versus time, showing their linear behaviours in precursory accelerations for three rock types. Response functions: $(\dot{R}_a / R_a - 1)^{-1}$ and $R_a \dot{R}_a^{-1}$.

data of $(\dot{R}_a/R_a - 1)^{-1}$ and $R_a\dot{R}_a^{-1}$. Figs. 5–7 show that the relationship of Eq. (20) is applicable earlier than the power-law relationship expressed by Eq. (17) or Eq. (1). Consequently, Eq. (20) can provide an earlier warning of catastrophe. Fig. 9 illustrates the predicted results in the time series obtained step-by-step using Eq. (20) for the three rock types. By comparison, the predicted results based on the power-law relationship in Eq. (17) are plotted in Fig. 9. In the predictions, only data close to the current time point were used, and future data were assumed to be unavailable. As expected, the predictions based on Eq. (17) at an earlier phase of the acceleration stage deviate significantly from the actual failure time; only those close to the catastrophic failure time represent good predictions. By contrast, the predictions obtained using Eq. (20) yield almost the same stable prediction, which agrees well with the actual failure times.

To quantitatively evaluate the prediction accuracy of the model, the relative error is defined as the ratio of the deviation of the predicted value U_P from the U_F value at the moment of destruction, which is used as a measure of the deviation of the predicted value from the true value; the closer the value is to zero, the smaller the deviation of the predicted value. This approach was used to determine the method that was more effective in predicting the time of catastrophe.

The curve representing the relative error versus U_t is shown in Fig. 10. It can be clearly seen that the relative error of the prediction error of Eq. (17) is large in the early acceleration section; when approaching the time of catastrophic failure, the value of the prediction relative error is close to zero, whereas the relative error of Eq. (20) is close to zero in the entire acceleration section.

6. Discussion

6.1. Catastrophic failure and precursory accelerations

The nonlinear evolution of failure in brittle rocks is defined by their intrinsic heterogeneous properties resulting from microdamage such as cracks and voids randomly distributed inside the bodies of the rocks. For an ideal homogeneous elastic-brittle material, the response quantities have a linear relationship with the controlling variable, and consequently, there is no precursory accelerating process (as shown in Fig. 11). The heterogeneity of brittle rocks produces a nonlinear acceleration process of deformation that evolves to a catastrophic point, as shown in Fig. 3. Therefore, heterogeneous mechanical behaviours, resulting from natural and random damage inside rock materials and the energy principle of catastrophic failure, define the precursory acceleration and singularity behaviour of the response functions, $R = \mathrm{d}\varepsilon/\mathrm{d}U$.

The acceleration of the failure approaching the catastrophic point can be attributed to damage localisation and energy release of the load apparatus. Damage accumulation in a shallow zone leads to rapid failure propagation. After the peak force, the deformation recovery of the elastic environment (e.g., the load apparatus in the experiments) resulting from unloading accelerates the deformation of the compressed specimen. Consequently, the increment in the deformation of a specimen is the sum of the increments of both the boundary displacement and the recovery deformation of the load apparatus, that is,

$$\mathrm{d}u = \mathrm{d}U - \mathrm{d}u_e \tag{23}$$

At the catastrophic point, an infinitesimal increase in the external control variable (U) results in a finite increase in the deformation response (u). Since $\mathrm{d}u_e$ is negative, its value is subtracted.

It is difficult to precisely determine the onset time when strain transitions to acceleration [2,20,30,31]. The initial point of the strain acceleration process was determined as the time after which the strain acceleration was at least one order of magnitude greater than the minimal (positive) value of acceleration.

6.2. Prediction and noise of acceleration

The heterogeneity of brittle rock and its complex evolution under a compression load leads to the sample specificity of catastrophic failure. Sample specificity is the main cause of uncertainty in the catastrophic failure times. The precursory acceleration process of the failure provides clues for predicting the failure time of an individual event.

How to determine the actual value of exponent β is a challenge that influences the accuracy of prediction based on the power-law relationship (Eq. (1)). The well-known inverse-rate method [6,10,11,17,19,22,32–34] and other methods [18,20] have been suggested to overcome this difficulty. The present description explains the prediction of the catastrophic failure time based on Eq. (20). This method does not require the critical exponent to be known beforehand. The catastrophic failure time was directly predicted by monitoring the time series data of $(\dot{R}_a/R_a - 1)^{-1}$. This applies earlier than the power-law relationship, and thus promises an earlier warning of catastrophic failure. It is noteworthy that Eqs. (20) and (21) indicate that the slope of the fitted line in Fig. 8 is equal to $1/\beta$. Consequently, β can be determined as the inverse slope.

The monitored data of both u and U in the experiments inevitably involve noise, which consequently causes fluctuations in the rates and accelerations calculated by differentiation. Fluctuations in the rate and acceleration data may lead to scatter in $(\dot{R}_a/R_a - 1)^{-1}$. Obviously, Eq. (18) describes the quasi-continuous evolution of the deformation acceleration. In practice, the evolution of deformation is a response to a time series of small, discrete, and intermittent damage events occurring in brittle rocks that are much smaller than macroscopic and catastrophic events. As time approaches the catastrophic point, the values of the deformation rates in response to damage events become large and increase rapidly, so the effects of noise can be suppressed. Consequently, noise had a smaller effect on the calculated values of the rates and accelerations in the final stage. Therefore, the precursory accelerations of the three types of rocks with different internal micro-structures are well described by Eq. (20). The internal micro-structures of the rocks should have a

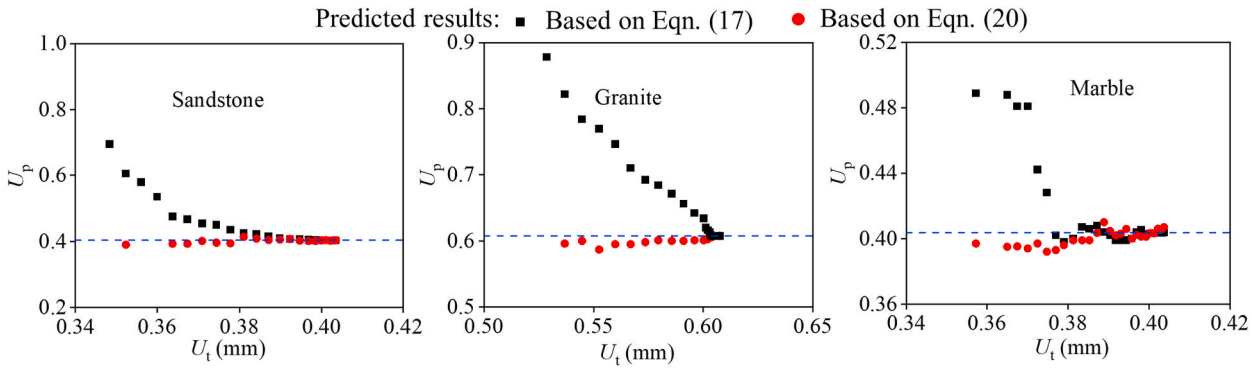

Fig. 9. Predicted results based on Eqs. (17) and (20), respectively. U_t is the real-time displacement at the current time point. U_P is the predicted value of U_F. The blue dashed line denotes the actual value of U_F. (For interpretation of the references to colour in this figure legend, the reader is referred to the Web version of this article.)

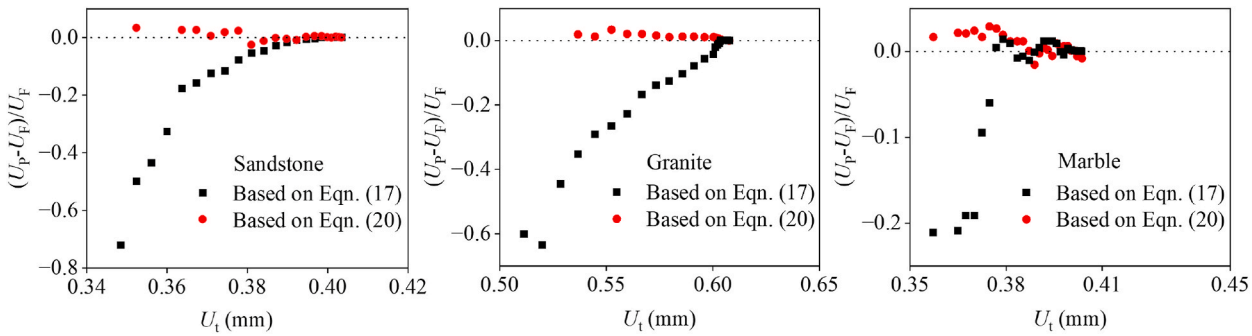

Fig. 10. Relative error versus U_t curve.

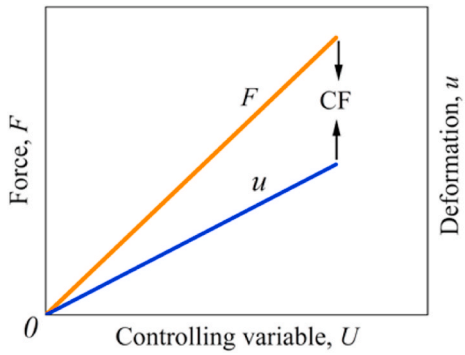

Fig. 11. Illustration of catastrophic failure (CF) of an ideal homogeneous material. No precursory acceleration appears ahead of the catastrophic failure.

significant influence on the duration of the precursory acceleration stage, the magnitudes of the strain rates and accelerations, the background noise, and the length (of time) ratio of the two phases in the precursory acceleration stage. Further investigations are needed to highlight the effects of the internal micro-structures. Furthermore, it should be noted that the present method for failure-time prediction must first determine the control variable (e.g., compressive displacement, U). This limits the application of the theoretical model when control variables are uncertain.

7. Conclusion

In this study, it was shown that an evident acceleration stage exists in the process of deformation evolving into the catastrophic failure of brittle rocks. The entire process of such acceleration failure comprises two phases. The data in the vicinity of the failure time

exhibit power-law behaviour with respect to the time to failure; however, the data in the earlier phase of the acceleration stage conform to an exponential function. Consequently, all data in the acceleration stage can be described well by a combination of exponential and power-law functions. A prediction method based on a combined description of the entire acceleration failure process can be used to forecast the failure time. This method was validated by experimental results for three types of rocks. The combined description of the entire acceleration failure process allows for an earlier warning of catastrophic failure than the well-established power law.

CRediT authorship contribution statement

Lei Cheng: Investigation, Methodology, Validation, Writing – original draft. **Shengwang Hao:** Conceptualization, Funding acquisition, Methodology, Supervision, Validation, Writing – original draft, Writing – review & editing. **Chunsheng Lu:** Conceptualization, Writing – review & editing. **Sunji Zhou:** Investigation, Methodology.

Declaration of competing interest

The authors declare that they have no known competing financial interests or personal relationships that could have appeared to influence the work reported in this paper.

Acknowledgements

This work was supported by the Hebei Natural Science Foundation (Grant No. D2020203001), the Key Research and Development Projects of Hebei Province (22375407D), and the National Natural Science Foundation of China (Grant No. 11672258).

References

[1] I.G. Main, Applicability of time-to-failure analysis to accelerated strain before earthquakes and volcanic eruptions, Geophys. J. Int. 139 (1999) F1–F6.
[2] M.J. Heap, P. Baud, P.G. Meredith, S. Vinciguerra, A.F. Bell, I.G. Main, Brittle creep in basalt and its application to time-dependent volcano deformation, Earth Planet Sci. Lett. 307 (2011) 71–82.
[3] H. Nechad, A. Helmstetter, R. El Guerjouma, D. Sornette, Creep ruptures in heterogeneous materials, Phys. Rev. Lett. 94 (2005).
[4] J.Z. Zhang, X.P. Zhou, Forecasting catastrophic rupture in brittle rocks using precursory AE time series, J. Geophys. Res. Solid Earth 125 (2020).
[5] R. Toussaint, S. Pride, Fracture of disordered solids in compression as a critical phenomenon. I. Statistical mechanics formalism, Phys. Rev. E 66 (2002) 036135.
[6] B. Voight, A method for prediction of volcanic eruptions, Nature 332 (1988) 125–130.
[7] H. Long, L.H. Liang, Y.G. Wei, Failure characterization of solid structures based on an equivalence of cohesive zone model, Int. J. Solid Struct. 163 (2019) 194–210.
[8] T. Carla, E. Intrieri, F. Traglia, T. Nolesini, G. Gigli, N. Casagli, Guidelines on the use of inverse velocity method as a tool for setting alarm thresholds and forecasting landslides and structure collapses, Landslides 14 (2017) 517–534.
[9] L.H. Liang, X.N. Li, H.Y. Liu, Y.B. Wang, Y.G. Wei, Power-law characteristics of damage and failure of ceramic coating systems under three-point bending, Surf. Coating. Technol. 285 (2016) 113–119.
[10] A.F. Bell, C.R.J. Kilburn, Precursors to dyke-fed eruptions at basaltic volcanoes: insights from patterns of volcano-tectonic seismicity at Kilauea volcano, Hawaii. B. Volcanol. 74 (2012) 325–339.
[11] C. Kilburn, Precursory deformation and fracture before brittle rock failure and potential application to volcanic unrest, J. Geophys. Res. Solid Earth 117 (2012).
[12] X.M. Fan, Q. Xu, J. Liu, S.S. Subramanian, C.Y. He, X. Zhu, L. Zhou, Successful early warning and emergency response of a disastrous rockslide in Guizhou province, China, Landslides 16 (2019) 2445–2457.
[13] R.R. Cornelius, P.A. Scott, A materials failure relation of accelerating creep as empirical description of damage accumulation, Rock Mech. Rock Eng. 26 (1993) 233–252.
[14] J. Vasseur, F.B. Wadsworth, M.J. Heap, I.G. Main, D.B. Dingwell, Does an inter-flaw length control the accuracy of rupture forecasting in geological materials? Earth Planet Sci. Lett. 475 (2017).
[15] A.F. Bell, M. Naylor, M.J. Heap, I.G. Main, Forecasting volcanic eruptions and other material failure phenomena: an evaluation of the failure forecast method, Geophys. Res. Lett. 38 (2011).
[16] S.W. Hao, F. Rong, M.F. Lu, H.Y. Wang, M.F. Xia, F.J. Ke, Y.L. Bai, Power-law singularity as a possible catastrophe warning observed in rock experiments, Int. J. Rock Mech. Min. 60 (2013) 253–262.
[17] Y. Lavallee, P.G. Meredith, D.B. Dingwell, K.U. Hess, J. Wassermann, B. Cordonnier, A. Gerik, J.H. Kruhl, Seismogenic lavas and explosive eruption forecasting, Nature 453 (2008) 507–510.
[18] J. Xue, S.W. Hao, J. Wang, F.J. Ke, C.S. Lu, Y.L. Bai, The changeable power law singularity and its application to prediction of catastrophic rupture in uniaxial compressive tests of Geomedia, J. Geophys. Res. Solid Earth 123 (2018) 2645–2657.
[19] B. Voight, A relation to describe rate-dependent material failure, Science 243 (1989) 200–203.
[20] S.W. Hao, H. Yang, D. Elsworth, An accelerating precursor to predict "time-to-failure" in creep and volcanic eruptions, J. Volcanol. Geoth. Res. 343 (2017) 252–262.
[21] S.W. Hao, C. Liu, C.S. Lu, D. Elsworth, A relation to predict the failure of materials and potential application to volcanic eruptions and landslides, Sci. Rep. 6 (2016).
[22] B. Voight, R.R. Cornelius, Prospects for eruption prediction in near real-time, Nature 350 (1991) 695–698.
[23] R.O. Salvage, J.W. Neuberg, Using a cross correlation technique to refine the accuracy of the failure forecast method: application to Soufriere Hills volcano, Montserrat, J. Volcanol. Geoth. Res. 324 (2016) 118–133.
[24] R. Smith, C.R.J. Kilburn, Forecasting eruptions after long repose intervals from accelerating rates of rock fracture: the June 1991 eruption of Mount Pinatubo, Philippines, J. Volcanol. Geoth. Res. 191 (2010) 129–136.
[25] J. Corcoran, Rate-based structural health monitoring using permanently installed sensors, P. Roy. Soc. A-Math. Phy. 473 (2017) 1–18.
[26] R.M. Robertson, C.R.J. Kilburn, Deformation regime and long-term precursors to eruption at large calderas: Rabaul, Papua New Guinea, Earth Planet Sci. Lett. 438 (2016) 86–94.
[27] A. Boué, P. Lesage, G. Cortes, B. Valette, G. Reyes-Davila, Real-time eruption forecasting using the material Failure Forecast Method with a Bayesian approach, J. Geophys. Res. Solid Earth 120 (2015) 2143–2161.
[28] A.F. Bell, M. Naylor, I.G. Main, The limits of predictability of volcanic eruptions from accelerating rates of earthquakes, Geophys. J. Int. 194 (2013) 1541–1553.
[29] J. Vasseur, F.B. Wadsworth, Y. Lavallée, A.F. Bell, I.G. Main, D.B. Dingwell, Heterogeneity: the key to failure forecasting, Sci. Rep. 5 (2015).

[30] B.T. Ngwenya, I.G. Main, S.C. Elphick, B.R. Crawford, B. Smart, A constitutive law for low-temperature creep of water-saturated sandstones, J. Geophys. Res. Solid Earth 106 (2001) 21811–21826.
[31] S.Q. Yang, Y.Z. Jiang, Triaxial mechanical creep behavior of sandstone, Min. Sci. Technol. 20 (2010) 339–349.
[32] R. Sparks, Forecasting volcanic eruptions, Earth Planet Sci. Lett. 210 (2003) 1–15.
[33] R. Smith, C.R.J. Kilburn, P.R. Sammonds, Rock fracture as a precursor to lava dome eruptions at mount St Helens from June 1980 to October 1986, Bull. Volcanol. 69 (2007) 681–693.
[34] C.R.J. Kilburn, B. Voight, Slow rock fracture as eruption precursor at Soufriere Hills Volcano, Montserrat. Geophys. Res. Lett. 25 (1998) 3665–3668.